

1 Inhibiting *Mycobacterium tuberculosis* CoaBC by targeting a new allosteric  
2 site.

3  
4 Vitor Mendes<sup>1\*</sup>, Simon R. Green<sup>2</sup>, Joanna C. Evans<sup>3</sup>, Jeannine Hess<sup>4</sup>, Michal Blaszczyk<sup>1</sup>,  
5 Christina Spry<sup>4</sup>, Owain Bryant<sup>1</sup>, James Cory-Wright<sup>1</sup>, Daniel S-H. Chan<sup>4</sup>, Pedro H.M.  
6 Torres<sup>1</sup>, Zhe Wang<sup>5</sup>, Sandra O'Neill<sup>2</sup>, Sebastian Damerow<sup>2</sup>, John Post<sup>2</sup>, Tracy Bayliss<sup>2</sup>,  
7 Sasha L. Lynch<sup>3</sup>, Anthony G. Coyne<sup>4</sup>, Peter C. Ray<sup>2</sup>, Chris Abell<sup>4</sup>, Kyu Y. Rhee<sup>5</sup>, Helena  
8 I. M. Boshoff<sup>6</sup>, Clifton E. Barry III<sup>3,6</sup>, Valerie Mizrahi<sup>3</sup>, Paul G. Wyatt<sup>2</sup>, Tom L.  
9 Blundell<sup>1\*</sup>.

10  
11 1 Department of Biochemistry, University of Cambridge, 80 Tennis Court Road, Cambridge, CB2 1GA,  
12 UK

13 2 Drug Discovery Unit, College of Life Sciences, University of Dundee, Dow Street, Dundee, DD1 5EH,  
14 Scotland, UK

15 3 MRC/NHLS/UCT Molecular Mycobacteriology Research Unit & DST/NRF Centre of Excellence for  
16 Biomedical TB Research & Wellcome Centre for Infectious Diseases Research in Africa, Institute of  
17 Infectious Disease and Molecular Medicine and Department of Pathology, Faculty of Health Sciences,  
18 University of Cape Town, Anzio Road, Observatory 7925, South Africa

19 4 Department of Chemistry, University of Cambridge, Lensfield Road, Cambridge, CB2 1EW, UK

20 5 Division of Infectious Diseases, Weill Department of Medicine, Weill Cornell Medical College, New  
21 York, NY 10065, USA

22 6 Tuberculosis Research Section, Laboratory of Clinical Immunology and Microbiology, National Institute  
23 of Allergy and Infectious Disease, National Institutes of Health, 9000 Rockville Pike, Bethesda, Maryland  
24 20892, USA

25

26 \* To whom correspondence should be addressed

27 Vitor Mendes: [vgm23@cam.ac.uk](mailto:vgm23@cam.ac.uk)

28 Tom L. Blundell: [tom@cryst.bioc.cam.ac.uk](mailto:tom@cryst.bioc.cam.ac.uk)

29 **Abstract**

30 Coenzyme A (CoA) is a fundamental co-factor for all life, involved in numerous  
31 metabolic pathways and cellular processes, and its biosynthetic pathway has raised  
32 substantial interest as a drug target against multiple pathogens including *Mycobacterium*  
33 *tuberculosis*. The biosynthesis of CoA is performed in five steps, with the second and  
34 third steps being catalysed in the vast majority of prokaryotes, including *M. tuberculosis*,  
35 by a single bifunctional protein, CoaBC. Depletion of CoaBC was found to be bactericidal  
36 in *M. tuberculosis*. Here we report the first structure of a full length CoaBC, from the  
37 model organism *Mycobacterium smegmatis*, describe how it is organised as a dodecamer  
38 and regulated by CoA thioesters. A high-throughput biochemical screen focusing on  
39 CoaB identified two inhibitors with different chemical scaffolds. Hit expansion led to the  
40 discovery of potent inhibitors of *M. tuberculosis* CoaB. Crucially, we further show that  
41 these compounds bind to a novel cryptic allosteric site within CoaB.

42

43

44

45

46

47

48

49

50

51

52

53

## 54 **Introduction**

55 Tuberculosis (TB) is the most prevalent and deadly infectious disease worldwide and  
56 remains a global epidemic. Despite the availability of treatment, this disease, caused by  
57 *Mycobacterium tuberculosis*, still claims 1.5 million lives each year <sup>1</sup>. Current treatment  
58 regimens are long, which presents an obstacle for patient adherence and imposes a heavy  
59 social and economic burden on countries with a high incidence of TB. It is therefore  
60 critical to explore novel targets and find new and more effective drugs to combat this  
61 disease.

62 Coenzyme A (CoA) is an essential and ubiquitous cofactor, involved in numerous  
63 metabolic pathways with a large number of different enzymes requiring it for activity<sup>2</sup>.  
64 CoA is essential for the synthesis of phospholipids, fatty acids, polyketides, and non-  
65 ribosomal peptides, for the operation of the tricarboxylic acid cycle and in the degradation  
66 of lipids <sup>3</sup>. The importance of CoA for essential post-translational modifications of  
67 proteins is also well established in both eukaryotes and prokaryotes with various proteins  
68 post-translationally modified by thioester derivatives of CoA (acylation) or CoA itself  
69 (phosphopantetheinylation and CoAlation), while several other post-translational  
70 modifications depend indirectly on CoA through the mevalonate pathway <sup>4-7</sup>.  
71 Furthermore, dephospho-CoA, an intermediate of the CoA pathway, is incorporated into  
72 some RNA transcripts during transcription initiation thereby serving as a non-canonical  
73 transcription initiating nucleotide <sup>8</sup>. These RNA modifications have functional  
74 consequences and occur in both eukaryotes and bacteria <sup>8</sup>. In *M. tuberculosis*, CoA plays  
75 a pivotal role in the biosynthesis of complex lipids that are crucial components of the cell  
76 wall and required for pathogenicity <sup>9</sup>. It is also needed for the degradation of lipids,  
77 including cholesterol, which are the primary source of energy for this organism during  
78 infection <sup>10,11</sup>. The CoA pathway is therefore an attractive pathway for drug discovery for

79 many different infectious diseases, including TB, given its ubiquitous nature, wide  
80 metabolic and functional impact of its inhibition and lack of sequence conservation  
81 between prokaryotes and humans.

82 The biosynthesis of CoA from pantothenic acid (vitamin B<sub>5</sub>) is performed in five steps,  
83 sequentially catalysed by the enzymes pantothenate kinase (CoaA, also known as PanK),  
84 phosphopantothenoylcysteine synthetase (CoaB), phosphopantothenoylcysteine  
85 decarboxylase (CoaC), phosphopantetheine adenylyltransferase (CoaD) and dephospho-  
86 CoA kinase (CoaE). However, in the vast majority of prokaryotes, including *M.*  
87 *tuberculosis*, CoaB and CoaC are encoded by a single gene to produce a fused  
88 bifunctional enzyme (CoaBC). Transcriptional silencing of individual genes of the CoA  
89 biosynthesis pathway of this pathogen identified CoaBC as uniquely bactericidal within  
90 the CoA pathway, highlighting it as a good candidate for drug discovery<sup>12</sup>.

91 CoaBC comprises two enzymes in a single polypeptide chain and converts 4'-  
92 phosphopantothenate to 4'-phosphopantetheine in three steps. First, 4'-  
93 phosphopantothenate (PPA) reacts with CTP to form 4'-phosphopantothenoyl-CMP with  
94 the release of pyrophosphate. This intermediate subsequently reacts with cysteine to form  
95 4'-phosphopantothenoylcysteine (PPC) with the release of CMP with these two steps  
96 being catalysed by CoaB. The product of CoaB is then decarboxylated by CoaC to 4'-  
97 phosphopantetheine an enzyme of the homo-oligomeric flavin-containing decarboxylase  
98 (HFCD) protein family. X-ray crystal structures have been reported for the individual  
99 CoaB and CoaC enzymes in several organisms, including a structure of CoaB from  
100 *Mycobacterium smegmatis*, a close relative of *M. tuberculosis* However, a structure of  
101 the full-length bifunctional CoaBC was missing.

102 Here we report the structure of the bifunctional CoaBC of *M. smegmatis* at 2.5 Å. We  
103 identify a previously unknown allosteric site in CoaB and crucially, we report the

104 identification of the first *M. tuberculosis* CoaBC allosteric inhibitors. Using X-ray  
105 crystallography and enzyme kinetic experiments, we define the mode of binding of one  
106 of the inhibitors and show its impact on the protein structure and function. These results  
107 further illustrate the potential of CoaBC as a novel drug target in *M. tuberculosis*.

108

## 109 **Results**

### 110 **Overall structure of CoaBC**

111 Because the HFCD protein family of flavin-binding proteins are known to form homo-  
112 oligomers<sup>13</sup>, we performed native electrospray-ionization mass spectrometry (ESI-MS)  
113 to investigate the stoichiometry of CoaBC, previously proposed to form a dodecamer<sup>13</sup>.  
114 Both *M. tuberculosis* CoaBC (MtbCoaBC) (Figure S1A) and *M. smegmatis* CoaBC  
115 (MsmCoaBC) (Figure S1B) exclusively exhibited a dodecameric assembly, with no other  
116 oligomeric species observed in the spectra, consistent with a strong interaction between  
117 the subunits of the complex. The dodecamer of MtbCoaBC was centred around the 56+  
118 charge state, with an observed mass of 537 kDa, while the dodecamer of MsmCoaBC was  
119 centred around the 52+ charge state, with an observed mass of 523 kDa. These masses  
120 are 1-2% higher than the expected masses of 525 and 518 kDa for MtbCoaBC and  
121 MsmCoaBC respectively, which can be attributed to the non-specific binding of solvent  
122 molecules or ions to the protein complexes under the soft ionization conditions employed.  
123 Structures of a few proteins of the HFCD family have been determined<sup>14-18</sup>. All of these  
124 structures show either a homo-trimeric or homo-dodecameric arrangement of the flavin-  
125 containing Rossmann-fold with trimers forming at each of the vertices of the tetrahedron  
126 in the case of a dodecameric arrangement<sup>15</sup>. However, all of these proteins, unlike  
127 CoaBC, contain only a single functional domain. We solved the structure of MsmCoaBC  
128 at 2.5 Å resolution (Figure 1A), in the presence of CTP and FMN (Figure 1B, S2A and

129 S2B), using crystals belonging to the  $H3_2$  space group with an asymmetric unit containing  
130 four protomers forming two CoaBC dimers. Data collection and refinement statistics are  
131 summarised in (Table S1). The final model (residues 2-412) covers both CoaC and CoaB,  
132 but densities for several residues in three loop regions in CoaB are not observed (residues  
133 290-298, 336-342, 363-376). However, all these residues except for 375 and 376 can be  
134 seen the MsmCoaB X-ray crystal structure (PDB: 6TH2) that we also solved in this work  
135 at 1.8 Å. The N-terminal CoaC of MsmCoaBC (residues 1-179) forms the same type of  
136 dodecameric arrangement seen in other HFCD family proteins such as the peptidyl-  
137 cysteine decarboxylase EpiD<sup>15</sup> and sits at the core of the dodecamer (Figure 1A and 1C)  
138 with the two domains connected through a small loop region (residues 180-189) that  
139 tightly interacts with both. The active site of CoaC sits at the interface between two  
140 protomers of the CoaC trimer and a protomer of an adjacent CoaC trimer with the FMN  
141 site facing inwards towards the hollow centre of the dodecamer (Figure 2A). A flexible  
142 flap that was observed before covering a reaction intermediate bound to *Arabidopsis*  
143 *thaliana* CoaC<sup>19</sup> is also observed in some of the protomers, but in an open conformation  
144 (Figure 1B).

145 The C-terminal CoaB of MsmCoaBC also displays a Rossmann fold consistent with the  
146 several other CoaB structures solved previously, including both the eukaryotic form, in  
147 which CoaB exists as an individual polypeptide, and the bacterial form where CoaB is  
148 typically fused with CoaC<sup>20-22</sup>. Each CoaB of MsmCoaBC (residues 190-414) dimerises  
149 with a CoaB belonging to an adjacent trimer (Figure 1C). The full protein resembles a  
150 tetrahedron with CoaB dimers positioned at the six edges and CoaC trimers at the four  
151 vertices (Figure 1A).

152 The shortest distance between a pair of CoaB and CoaC active sites is ~30 Å (Figure 2B).  
153 Nevertheless, a flexible loop (residues 362-377) that covers the 4'-phosphopantothenate

154 site when this substrate binds to the enzyme <sup>20</sup> can be seen in our MsmCoaB structure,  
155 extending away from the active site. A superposition of our MsmCoaB dimer structure  
156 with MsmCoaBC shows the loop extending towards the CoaC active site (Figure 2B).  
157 This long loop (15-16 amino acids) is present in all CoaBCs (Figure S3) and it is possible  
158 that it helps channel the substrate from the CoaB to the CoaC active site.

159 The small differences (RMSD = 1.147) in overall structure of CoaB dimers in the full  
160 length MsmCoaBC and the MsmCoaB crystal structure solved at 1.8 Å (PDB: 6TH2) can  
161 be attributed to artefacts of crystal packing (Figure S4). Similarly, the CoaC structure  
162 does not seem to differ between full length MsmCoaBC and the available individual CoaC  
163 structures. However, when MsmCoaB (residues 186-414) is expressed alone, the protein  
164 does not dimerise in solution and is inactive (not shown). This contrasts with *E. coli*  
165 CoaB, which still dimerises and is functional when expressed on its own without the N-  
166 terminal CoaC <sup>23,24</sup>. The CoaB dimer interface is mostly conserved, but there are clear  
167 differences in the dimerisation region between MsmCoaB and *E. coli* CoaB that could  
168 help to explain the different observed behaviours (Figure S3). The absence of  
169 dimerization for the MsmCoaB when expressed alone suggests that the interactions  
170 between CoaC and CoaB in *M. smegmatis*, and likely all other *Mycobacteriaceae*, are  
171 fundamental for CoaB dimerisation and activity. This idea is reinforced by the fact that  
172 the residues located at the interface of the two enzymes (CoaB and CoaC) are well  
173 conserved in all *Mycobacteriaceae* and somewhat conserved in the sub-order  
174 *Corynebacterineae* but not outside of this group (Figure S3).

175 The CoaB dimerisation region forms a  $\beta$ -sandwich composed of eight anti-parallel  $\beta$ -  
176 strands, related by 2-fold symmetry, that contacts with the active site (Figure 2C and 2D).  
177 Comparison of the MsmCoaB with human CoaB reveals that the human and many other

178 eukaryotic CoaBs <sup>21</sup> possess two extra  $\alpha$ -helices and  $\beta$ -strands involved in the  
179 dimerisation interface that help stabilise the dimer in the absence of CoaC (Figure S5).  
180 The CoaB active site is enclosed by a loop that extends from the opposing protomer and  
181 is observed for the first time in this work. This loop contains a motif “K-X-K-K”, which  
182 is widely conserved in bacteria (Figure S3), with few exceptions, and each lysine either  
183 interacts directly with the triphosphate group of CTP or through highly coordinated  
184 waters (Figure 2C). Also observed for the first time is the coordination of a cation by the  
185 triphosphate group and D281 (Figure 2C and S6). While magnesium or manganese are  
186 the favoured cations for CoaB activity <sup>25</sup>, calcium is observed in our structures instead,  
187 due to the high concentration present in the crystallization condition.

188

### 189 **CoaBC is regulated by CoA thioesters**

190 It is known that CoA biosynthesis is regulated, in many organisms, at the first step of the  
191 pathway, catalysed by the enzyme CoaA <sup>3</sup>. *M. tuberculosis* and many other mycobacteria  
192 possess two isoforms of this enzyme (type I and III), however only the type I isoform  
193 seems to be active based on studies in *M. tuberculosis* <sup>26</sup>. CoA and its thioesters  
194 competitively inhibit this enzyme by binding to the ATP site with CoA being the strongest  
195 regulator <sup>27,28</sup>. Nevertheless, at physiologically relevant levels of CoA there is only a low  
196 level inhibition of CoaA <sup>28</sup>. It is also known that CoaD, the enzyme that catalyses the  
197 fourth step of the pathway, is competitively inhibited by CoA and its product dephospho-  
198 CoA <sup>29,30</sup>. However, nothing was known about the regulation of CoaBC. We therefore  
199 examined the effect of CoA and several of its thioesters (acetyl-CoA, malonyl-CoA and  
200 succinyl-CoA) on MtbCoaBC activity, using a coupled enzymatic assay that quantifies  
201 the release of pyrophosphate (EnzCheck pyrophosphate assay). Controls performed to



202 assess the activity of these compounds against the two coupling enzymes and the  
203 compounds showed an absence of inhibition at the tested range of concentrations.  
204 Potent regulation of CoaB activity by CoA and acyl-CoAs was observed, with IC<sub>50</sub> values  
205 ranging from 38 to 148 μM, far below the predicted intracellular concentrations of acyl-  
206 CoAs<sup>31</sup>, with succinyl-CoA displaying the highest inhibition (Figure 3A and Table 1).  
207 Competition assays with the three substrates and acetyl-CoA show a competitive mode  
208 of inhibition relative to CTP and PPA, and non-competitive inhibition for L-cysteine  
209 (Figure 3B). In the absence of a crystal structure to confirm the mode of binding, these  
210 results suggest that acyl-CoAs most likely bind to the active site itself, competing directly  
211 with CTP and PPA. Interestingly both acyl-CoAs, involved in fatty acid synthesis, as well  
212 as those, involved in the TCA cycle, show inhibition of CoaB with larger fatty acyl chains  
213 showing higher inhibition of CoaB.

214

### 215 **Identification of CoaB inhibitors using high-throughput screening**

216 Although the CoA biosynthetic pathway is considered an attractive target for drug  
217 discovery, CoA pathway inhibitors displaying potent whole cell activity are rare and the  
218 few CoaBC inhibitors that have been reported to date are in majority substrate mimicking  
219 <sup>24,32</sup>.

220 In order to identify novel MtbCoaBC inhibitors, we have conducted a high-throughput  
221 screen of 215,000 small molecules targeting CoaB activity. To do this an end-point  
222 pyrophosphate quantification assay was used (Biomol Green). The most potent hits  
223 identified were compounds **1a** and **2a** with IC<sub>50</sub> values of 9 and 3.1 μM respectively  
224 (Table S2), originating from two different but related chemical scaffolds. A search was  
225 then performed for commercially available analogues. Testing of analogues of the initial  
226 hits resulted in the identification of more potent compounds with sub-micromolar IC<sub>50</sub>

227 values (Table 1, Figure 4A, Table S2 and Figure S7). Of these, compounds **1b** and **2b**  
228 (Figure 4A and Table 1), with IC<sub>50</sub> values of 0.28 and 0.08 μM respectively, were  
229 identified as the most potent of the two chemical series and therefore were selected for  
230 further work.

231

### 232 **Elucidation of the mode of inhibition**

233 Following the identification of potent MtbCoaB inhibitors we went on to determine their  
234 mode of inhibition using kinetic assays. For this, the EnzCheck coupled enzyme assay  
235 that measures the release of pyrophosphate was used. Control experiments were first  
236 performed to assess compound activity against the two coupling enzymes and the  
237 compounds were found to be inactive at 100 μM. The IC<sub>50</sub> values for the compounds  
238 against CoaB were reassessed with this assay and the values obtained were in line with  
239 the primary screening assay (Table S2).

240 Competition experiments were then performed using the three CoaB substrates for the  
241 two most potent compounds of each chemical series (**1b** and **2b**). Compound **1b** was  
242 found to preferentially bind to the enzyme-substrate complex with uncompetitive  
243 inhibition observed for all substrates (Figure 4B), consistent with the compound binding  
244 preferentially when the three substrates are bound. Compound **2b** shows mixed inhibition  
245 relative to CTP and uncompetitive inhibition for L-cysteine and PPA (Figure 4C). It is  
246 known that CoaB forms the phosphopantothenoil-CMP intermediate in the absence of L-  
247 cysteine<sup>33</sup> and it is likely, due to spatial constraints, that cysteine can only bind at the  
248 active site after the release of pyrophosphate. The data is therefore consistent with  
249 compound **1b** preferentially binding after L-cysteine enters the active site, for to the last  
250 step of catalysis and the formation of 4'-phosphopantothenoilcysteine and CMP.  
251 However, compound **2b** shows a mixed inhibition for CTP, reflecting a slightly different

252 mechanism of action. These results obtained for both compounds suggest the existence  
253 of an allosteric site in the CoaB moiety of MtbCoaBC.

254

### 255 **Structural basis for inhibition of CoaB by allosteric inhibitors**

256 In order to elucidate the binding mode of compound **1b** we used a truncation of the  
257 MsmCoaB (residues 187-414) that was previously crystallized before by others in the  
258 presence of CTP (PDB code: 4QJI) at 2.65 Å resolution. The screening for new  
259 crystallization conditions allowed us to find a new CTP containing condition that gave  
260 excellent resolution (1.8 Å). Comparison of this structure with the full length MsmCoaBC  
261 showed only minor differences that can be attributed to crystal packing (Figure S4).  
262 Hence this crystallization system could be used to validate CoaB inhibitors binding  
263 outside of the CTP site.

264 MsmCoaB was co-crystallized with CTP in the absence of compound **1b** and overnight  
265 soaking of the crystals with this compound was performed. A Co-crystal structure of  
266 MsmCoaB with compound **1b** was obtained and showed that the compound was bound  
267 to a site at the dimer interface of CoaB, in a deep cavity that is occluded when the  
268 compound is absent (Figure 5A-B and S8). Each CoaB dimer contains two of these sites,  
269 which are formed by a sandwich of eight β-strands and a long loop that contains the  
270 conserved “K-X-K-K” motif. This site opens to the active site and the inhibitor also  
271 contacts with D281 that is involved in the coordination of the cation (Figure 5C). The  
272 opening/closing of this cryptic allosteric site is mediated by the side chain of R207 of the  
273 opposing protomer (Figure 5D) that moves 5.5 Å at the furthest point and to a smaller  
274 extent by the side chain of F282 that moves 2 Å. R207 has previously been shown to be  
275 critical for the second half of the reaction catalysed by CoaB, the conversion of the 4’-  
276 phosphopantothenoyl-CMP intermediate to PPC, with almost no conversion of the

277 intermediate to *PPC* detected when this arginine is mutated to glutamine<sup>33</sup>. Given the  
278 position of this arginine, it is likely that it is involved in the binding of cysteine. Despite  
279 the absence of a crystal structure with cysteine, kinetic data showing uncompetitive  
280 inhibition with cysteine is consistent with this.

281 This allosteric site is comprised of a large group of hydrophobic residues (I209, F282  
282 L304 of protomer A and L203, I292, P299 and I302 of protomer B) many of which form  
283 hydrophobic interactions with compound **1b** (Figure 5C). Several  $\pi$ -interactions between  
284 the compound and the protein are also observed and involve D281 and F282 of protomer  
285 A and R207 of protomer B (Figure 5D). Hydrogen-bond interactions are formed with  
286 D281 and F282 of protomer A and R207 of protomer B. Water-mediated interactions are  
287 also observed for a group of residues that sit at the outer edge of the site (L203, H286 and  
288 D303) that is formed exclusively by protomer B (Figure 5C).

289 We propose that upon binding of L-cysteine, the R207 side chain moves towards the  
290 active site, and is likely involved in stabilizing/orienting L-cysteine to attack the  
291 phosphopantothenoil-CMP intermediate. This movement opens the allosteric site, which  
292 allows binding of allosteric inhibitors to the newly created cavity. The allosteric inhibitors  
293 will then stabilize the enzyme in its substrate bound state with the position of R207  
294 becoming locked by several hydrogen-bonds with the side chain of D281 of protomer A,  
295 the backbone carbonyl group of I292 and the side chain of D204 of protomer B but also  
296 by the  $\pi$ -interactions with the compound (Figure 5C). The residues around this site and  
297 crucially R207 are conserved across many microorganisms, suggesting that this allosteric  
298 site is present in most, if not all bacterial CoaBCs (Figure S3 and S9A). Interestingly,  
299 even though overall sequence identity is very low between the human CoaB and  
300 MsmCoaB (22%), the human enzyme also contains an arginine equivalent to R207 and a

301 roughly similar interface with several conserved residues, but there are stark differences  
302 in the relative position of the residues at this site between the two enzymes (Figure S9B).  
303 While we were not able to obtain co-crystal structures with other inhibitors, *in silico*  
304 docking helped to provide a possible explanation for the structure-activity relationship  
305 observed for series one and two. The highest-scoring docking pose of compound **1b** the  
306 most potent inhibitor of series one, was almost identical to that observed in the co-crystal  
307 structure (Figure S10A), and the analogues for which docking was performed adopted a  
308 similar binding pose. The lower activity of compound **1a** relative to compound **1b** could  
309 be explained by the loss of water-mediated hydrogen bonds (Figure 5C, S10B), while the  
310 lower activity of compound **1c** could be explained by the loss of the carbonyl group which  
311 faces a highly electropositive area of the protein (Figure S10C). Compound **2b** is  
312 predicted to form direct hydrogen bonds at the bottom of the allosteric site, similar to  
313 those formed by compound **1b** but also to interact directly with L203 and H286, forming  
314 extra hydrogen bonds at the top of the allosteric site (Figure 6). For compound **1b** the  
315 interactions at the top of the site are water mediated (Figure 5C). This could explain the  
316 higher potency of compound **2b**. Compounds **2c** and **2d** are also predicted to form direct  
317 hydrogen bond interactions at the top of the allosteric site, but the interactions at the  
318 bottom of the site are not as favourable due to the presence of extra hydroxyl groups  
319 (Figure S10D-F). The remaining compounds in series two, which have fewer hydroxyl  
320 groups and/or with hydroxyl groups in different positions, lose the ability to form  
321 hydrogen bonds, consistent with the weaker inhibitory effect observed (Table S2).

322

### 323 **Screening of CoaBC inhibitors against *M. tuberculosis***

324 The *in vitro* whole cell activity of the compounds was further evaluated by their ability  
325 to inhibit *M. tuberculosis* growth on different carbon sources. None of the compounds

326 exhibited activity in media containing glycerol or cholesterol as the main carbon source.  
327 We then tested whether the lack of inhibitory activity could be attributed to the presence  
328 of BSA by determining the whole cell activity of the three most potent inhibitors against  
329 *M. tuberculosis* in GAST/Fe minimal media. All the tested compounds exhibited  
330 moderate to low activity in this media with compound **2b** displaying the best activity of  
331 the three (Table 2). The observed differences in potency between the enzymatic assay and  
332 whole cell activity are likely related to low compound permeation, high efflux or  
333 metabolisation.

334

### 335 **Discussion**

336 CoA is an essential co-factor ubiquitous in all domains of life. For many years, this  
337 pathway has been considered an attractive drug target to develop new antibiotics against  
338 a wide range of pathogens including *M. tuberculosis*. Furthermore, the recent  
339 identification of CoaBC as a key fragility point in the CoA pathway of this organism<sup>12</sup>,  
340 combined with the extremely low sequence identity with the human CoaB (25%) makes  
341 this enzyme an highly attractive drug discovery target.

342 However, we were aware that the many questions remaining at the start of this work about  
343 the organization and regulation of this bi-functional enzyme could have significant  
344 implications for drug discovery. We therefore set out to obtain a full-length structure of  
345 a CoaBC from mycobacteria and we were successful in solving the full length  
346 MsmCoaBC but also MsmCoaB alone, which share very high sequence identity with the  
347 *M. tuberculosis* orthologue (86% full-length, 84% CoaB enzyme) and hence valuable  
348 tools for studying *M. tuberculosis* CoaBC. The CoaBC organization we revealed is  
349 similar to other HFCD family proteins<sup>15</sup> but unique in the sense that it contains more than

350 one domain and highlights how the arrangement of the fused enzymes is essential for  
351 mycobacterial CoaB dimerisation and function.

352 Regulation of the CoA biosynthesis pathway by its product (CoA) was known to occur  
353 for other enzymes of the pathway but no information was available for CoaBC. We  
354 demonstrate that both CoA as well as several CoA thioesters regulate CoaBC by  
355 inhibiting CoaB activity with succinyl-CoA showing the greatest inhibition of the tested  
356 acyl-CoAs, and that these molecules act in a competitive manner with CTP and PPA and  
357 a non-competitive manner with L-cysteine. This is consistent with these molecules  
358 binding to the CoaB active site but not to the L-cysteine sub-site.

359 CoA and acyl-CoAs inhibit both CoaA and CoaD enzymes to varying extents <sup>28,30,34</sup>.  
360 However, the inhibitory effect of CoA and its thioesters in their activity is low when  
361 compared to what we observed in CoaBC and consequently the impact of the intracellular  
362 level of these molecules will be higher in CoaBC . We therefore report a new and  
363 important mechanism of regulation of de novo CoA biosynthesis, mediated by the action  
364 of CoA thioesters on CoaBC. Since the reported intracellular levels of these molecules <sup>31</sup>  
365 are normally above the observed IC<sub>50</sub> the activity of CoaBC is highly inhibited. This  
366 correlates well with previous work showing that “de novo” CoA biosynthesis closely  
367 matches dilution due to cell division <sup>35</sup>. However, the data for intracellular concentrations  
368 of CoA and CoA thioesters as well CoA half-life was not obtained for mycobacteria and  
369 both interspecies differences as well as variations in growth conditions may affect these  
370 conclusions.

371 Although the CoA pathway and CoaBC have been the subject of many drug discovery  
372 efforts, few non-substrate-mimicking inhibitors of CoaBC have been reported <sup>24</sup>. Our  
373 work identifies two related chemical scaffolds that potently inhibit the activity of the  
374 CoaB moiety of MtbCoaBC through a new cryptic allosteric site that sits in the dimer

375 interface region of the CoaB enzyme. This site is closed in the CTP-bound structure, by  
376 the side chain of R207 a residue known to be involved in the second and final step of the  
377 reaction catalysed by CoaB – the conversion of the 4'-phosphopantothenoyl-CMP  
378 intermediate to PPC<sup>33</sup>. Considering the role of this in the final step of product formation  
379 and that compound **1b** shows uncompetitive inhibition relative to all CoaB substrates, we  
380 propose that the opening of this site occurs upon binding of the final substrate L-cysteine.  
381 Currently it is not clear whether this new allosteric site is exploited by a natural ligand,  
382 as we were unable to identify such a biomolecule. Nevertheless, the conservation of  
383 residues at this site, across a variety of bacteria, indicates that this feature might be  
384 common to many, if not all, bacterial CoaBs.

385 Drug discovery against *M. tuberculosis* is rich in examples of compounds with potent  
386 activity against an essential enzyme but with a complete lack of whole cell activity due  
387 to the impermeable cell wall of this organism, efflux pumps, target modification enzymes  
388 and extensive capacity to metabolise compounds<sup>36</sup>. The lack of in vitro whole cell activity  
389 displayed by the CoaB inhibitors reported in this work, may relate to any of these issues.  
390 However, the activity observed in albumin free media (GAST media) also points to the  
391 possibility of compound binding to albumin interfering with the assay. Nevertheless, the  
392 promising biochemical and structural data described herein further validates CoaBC as a  
393 promising novel anti-tubercular drug target by showing a new allosteric site that can be  
394 targeted by potent inhibitors.

395

## 396 **Materials and methods**

### 397 **Cloning and protein purification**

398 *Mycobacterium tuberculosis* and *Mycobacterium smegmatis* *coaBC* genes were amplified  
399 from genomic DNA of *M. tuberculosis* H37Rv strain, obtained from ATCC



400 (ATCC25618D-2) and genomic DNA of *M. smegmatis* mc<sup>2</sup> 155 (graciously provided by  
401 Dr. Nuno Empadinhas), and cloned into a pET28a vector (Novagen), modified to include  
402 an N-terminal 6xHis-SUMO tag. *M. smegmatis* *coaB* construct was obtained from Seattle  
403 Structure Genomics Center for Infectious Disease. The same protein purification protocol  
404 was used for both *M. tuberculosis* and *M. smegmatis* CoaBC constructs.

405 *E. coli* BL21(DE3) containing pET28aSUMO-CoaBC was grown in 2XYT media at 37  
406 °C until an O.D.<sub>600</sub> = 0.6. IPTG was then added to a final concentration of 0.5 mM at the  
407 temperature changed to 18 °C for 18-20h. Cells were then harvested by centrifugation, re-  
408 suspended in 50 mM TRIS pH 8.0, 250 mM NaCl, 20% (w/v) glycerol, 20 mM imidazole,  
409 5 mM MgCl<sub>2</sub> with protease inhibitors tablets (Roche) and DNaseI (Sigma). Cells were  
410 lysed with an Emulsiflex (Avestin) and the resultant cell lysate was centrifuged at 27000  
411 x g for 30 min to remove cell debris. Recombinant CoaBCs were purified with a HiTrap  
412 IMAC Sepharose FF column (GE-Healthcare), equilibrated with 50 mM TRIS pH 8.0,  
413 250 mM NaCl, 20% glycerol (w/v) and 20mM Imidazole. Elution was performed in the  
414 same buffer with 500mM Imidazole. Protein was dialysed in 25 mM TRIS pH 8 and 150  
415 mM and SUMO tag was cleaved overnight at 4 °C by adding Ulp1 Protease at 1:100  
416 ratio. CoaBC was concentrated and loaded in a Superdex 200 column equilibrated with  
417 25mM TRIS pH 8.0, 150 mM NaCl. Fraction purity was determined by SDS-page and  
418 the purest fractions were pooled, concentrated to ~10 mg.ml<sup>-1</sup> for *M. tuberculosis* CoaBC  
419 and 30 mg.ml<sup>-1</sup> for *M. smegmatis* CoaBC, flash frozen in liquid nitrogen and stored at -  
420 80 °C.

421 *E. coli* BL21(DE3) containing the *M. smegmatis* CoaB construct with a N-terminal non-  
422 -cleavable 6xhis tag was grown and harvested as above and re-suspended in 20 mM  
423 HEPES pH 7.0, 500 mM NaCl, 20 mM imidazole, 5 mM MgCl<sub>2</sub> with protease inhibitors  
424 tablets (Roche) and DNaseI (Sigma). Cells were lysed with an Emulsiflex (Avestin) and

425 cell lysate was centrifuged at 27000 g for 30 mins to remove cell debris. Recombinant *M.*  
426 *smegmatis* CoaB was purified with a HiTrap IMAC Sepharose FF column (GE-  
427 Healthcare), equilibrated with 20 mM HEPES pH 7.0, 500 mM NaCl and 20 mM  
428 imidazole. Elution was carried in the same buffer with 500 mM imidazole. Protein was  
429 concentrated and loaded on a Superdex 200 column equilibrated with 20mM HEPES pH  
430 7.0 and 500 mM NaCl. Fraction purity was assessed by SDS-page and the purest fractions  
431 were pooled concentrated to 22 mg. ml<sup>-1</sup>, flash frozen in liquid nitrogen and stored at -80  
432 °C.

433

#### 434 **Native mass spectrometry**

435 Spectra were recorded on a Synapt HDMS mass spectrometer (Waters) modified for  
436 studying high masses. MtCoaBC and MsCoaBC were exchanged into NH<sub>4</sub>OAc (500 mM,  
437 pH 7.0) solution using Micro Bio-Spin 6 chromatography columns (Bio-Rad). 2.5 µL of  
438 sample solution was injected into a borosilicate emitter (Thermo Scientific) for sampling.  
439 Instrument conditions were optimized to enhance ion desolvation while minimizing  
440 dissociation of macromolecular complexes. Typical conditions were capillary voltage  
441 1.8–2.0 kV, sample cone voltage 100 V, extractor cone voltage 1 V, trap collision voltage  
442 60 V, transfer collision voltage 60 V, source temperature 20 °C, backing pressure 5 mbar,  
443 trap pressure 3–4 × 10<sup>-2</sup> mbar, IMS (N<sub>2</sub>) pressure 5–6 × 10<sup>-1</sup> mbar and TOF pressure 7–  
444 8 × 10<sup>-7</sup> mbar. Spectra were calibrated externally using cesium iodide. Data acquisition  
445 and processing were performed using MassLynx 4.1 (Waters).

446

#### 447 **Crystallization**

448 For both full length *M. smegmatis* CoaBC and CoaB alone, the crystallization screens and  
449 optimization were performed at 18 °C using the sitting-drop vapour diffusion method. For

450 CoaBC 300 nL of pure protein at 30 mg.ml<sup>-1</sup>, pre-incubated with 3 mM CTP and 10 mM  
451 MgCl<sub>2</sub>, was mixed in 1:1 and 1:2 (protein to reservoir) ratio with well solution using a  
452 mosquito robot (TTP labtech). Initial conditions were obtained in the Classics lite  
453 crystallization screen (Qiagen), solution 1. Crystals obtained in this condition diffracted  
454 poorly, therefore several rounds of optimization were performed. The final optimised  
455 condition consisted of 0.1 M BisTris pH 6.5, 10 mM CoCl<sub>2</sub> 0.8 M 1,6-hexanediol.  
456 Crystals appeared after three days in both conditions. A cryogenic solution was prepared  
457 by adding ethylene glycol up to 30% (v/v) to mother liquor. Crystals were briefly  
458 transferred to this solution, flash frozen in liquid nitrogen and stored for data collection.  
459 For MsmCoaB 200 nL of pure protein at 22-24 mg.mL<sup>-1</sup> with 10 mM CTP was mixed in  
460 1:1 ratio with well solution using a Phoenix robot (Art Robbins). Crystals were obtained  
461 in Wizards classics III&IV (Rigaku) solution G4 consisting of 20% (w/v) PEG 8000,  
462 0.1M MES pH 6.0 and 0.2 M calcium acetate. Crystals appeared after 2 days.  
463 To obtain ligand-bound structures, soaking was performed condition using the hanging-  
464 drop vapour-diffusion method as follows: 2 uL of a solution containing 20% (w/v) PEG  
465 8000, 0.1M MES pH 6.0, 0.2 M calcium acetate, 0.25 M NaCl 10% (v/v) DMSO and 1-  
466 5 mM inhibitors was left to equilibrate against 500 µl of reservoir solution for 3 days.  
467 Crystals were then transferred to the pre-equilibrated drops and incubated for 24h. A  
468 cryogenic solution was prepared by adding 2-Methyl-2,4-pentanediol up to 25% (v/v) to  
469 mother liquor. Crystals were briefly transferred to this solution, flash frozen in liquid  
470 nitrogen and stored for data collection.  
471 While we have also obtained *M. tuberculosis* CoaBC crystals they did not diffract and  
472 our optimization efforts failed to improve them.

473

474 **Data collection and processing**

475 The data sets were collected at stations I02 and I03 at Diamond Light Source (Oxford,  
476 UK). The diffraction images were processed with AutoPROC <sup>37</sup> using XDS <sup>38</sup> for  
477 indexing and integration with AIMLESS <sup>39</sup> and TRUNCATE <sup>40</sup> from CCP4 Suite <sup>41</sup> for  
478 data reduction, scaling and calculation of structure factor amplitudes and intensity  
479 statistics.

480

### 481 **Structure solution and refinement**

482 MsmCoaB and MsmCoaBC structures were solved by molecular replacement using  
483 PHASER <sup>42</sup> from the PHENIX software package <sup>43</sup>. For MsmCoaB the atomic  
484 coordinates of MsmCoaB structure (PDB entry 4QJI) were used as a search model.  
485 Ligand bound structures were solved using our highest resolution MsmCoaB apo form  
486 structure (PDB entry 6TH2). For MsmCoaBC atomic coordinates of *Arabidopsis thaliana*  
487 CoaC (PDB entry 1MVL) <sup>19</sup> and our highest resolution CoaB structure (PDB entry 6TH2)  
488 were used as search models. Model building was done with Coot <sup>44</sup> and refinement was  
489 performed in PHENIX <sup>43</sup>. Structure validation was performed using Coot and PHENIX  
490 tools <sup>43,44</sup>. All figures were prepared using Pymol (The PyMOL Molecular Graphics  
491 System, Version 2.0 Schrödinger, LLC.) and ligand interactions calculated with Arpeggio  
492 <sup>45</sup>.

493

### 494 **High-throughput screening**

495 Potential inhibitors of CoaBC were assessed at room temperature using a PHERAStar  
496 microplate reader (BMG Labtech). Pyrophosphate produced by CoaB was converted to  
497 two molecules of inorganic phosphate using a pyrophosphatase. Phosphate was then  
498 detected using the BIOMOL® Green reagent (Enzo Life Sciences), which when bound  
499 to phosphate absorbs light at 650 nm. An end-point assay was carried out in clear, flat-

500 bottom, polystyrene, 384-well plates (Greiner) in an 50  $\mu$ l reaction volume containing  
501 100 mM TRIS, pH 7.6; 1 mM  $MgCl_2$ ; 1 mM TCEP; 0.03 U/mL pyrophosphatase; 2  $\mu$ M  
502 CTP; 40  $\mu$ M L-cysteine; 30  $\mu$ M PPA and 30 nM MtbCoaBC. Assays were performed by  
503 adding 25  $\mu$ L of a 2-times concentrated reaction mixture containing all components with  
504 the exception of the enzymes to all wells, and the reactions started by adding 25  $\mu$ L of a  
505 2-times concentrated enzyme mixture. The reaction was carried out for 2 h at room  
506 temperature, before 50  $\mu$ L of BIOMOL® Green reagent was added and incubated for a  
507 further 20 min prior to reading.

508

509 **Inorganic pyrophosphatase-purine nucleoside phosphorylase PNP-PPIase assay.**

510 The commercially available EnzCheck pyrophosphate assay kit (E-6645) (Life  
511 Technologies) was used for this assay. The final reaction composition used was 0.03  
512 U/mL inorganic pyrophosphatase, 1 U/mL purine nucleoside phosphorylase, 1 mM  
513  $MgCl_2$ , 200  $\mu$ M MESG, 100 mM TRIS pH 7.5, 1 mM TCEP, 32 nM MtbCoaBC, 125  
514  $\mu$ M CTP, 125  $\mu$ M PPA, 500  $\mu$ M L-cysteine, and various concentrations of compounds  
515 being tested for inhibition all prepared from DMSO stock solutions (compounds of series  
516 one and two) or water (CoA and CoA thioesters). Assays were performed on either a  
517 CLARIOStar or PHERAStar microplate reader (BMG Labtech) in 96-well plates  
518 (Greiner). A substrate mixture containing the substrates and the inhibitor was pre-  
519 incubated at 25 °C for 10 min. An enzyme solution was prepared and separately pre-  
520 incubated at 25 °C for 10 min. The reaction was initiated by the addition of the substrates  
521 to the solution containing the enzyme to a final volume of 75  $\mu$ L. Enzymatic activity was  
522 monitored by following the absorbance at 360 nm for 30 min (100 cycles/20 s each cycle).  
523 Assays were performed in triplicates, including a negative control (lacking PPA) and a  
524 positive control (lacking inhibitor).

525 Competition assays were performed using the same conditions but with variable substrate  
526 concentrations (31.25  $\mu$ M, 62.5  $\mu$ M, 125  $\mu$ M, 250  $\mu$ M and 500  $\mu$ M for CTP and PPA,  
527 31.25  $\mu$ M, 62.5  $\mu$ M, 93.75  $\mu$ M 125  $\mu$ M and 250  $\mu$ M for L-cysteine).

528

#### 529 ***M. tuberculosis* strains and growth conditions**

530 MIC determination for *M. tuberculosis* H37RvMA was performed as previously  
531 described<sup>46</sup> in the following media: 7H9/ADC/glycerol (4.7 g/L Difco Middlebrook 7H9  
532 base, 100mL/L Middlebrook albumin (BSA)-dextrose-catalase (ADC) Difco  
533 Middlebrook, 0.2% glycerol and 0.05% Tween-80) , 7H9/Cholesterol/Tyloxapol (4.7 g/L  
534 7H9 base, 0.81 g/L NaCl, 24 mg/L cholesterol, 5 g/L BSA fraction V and 0.05%  
535 Tyloxapol), GAST/Fe (0.3 g/L of Bacto Casitone (Difco), 4.0/L g of dibasic potassium  
536 phosphate, 2.0 g/L of citric acid, 1.0 g/L of L-alanine, 1.2 g/L of magnesium chloride  
537 hexahydrate, 0.6 g/L of potassium sulfate, 2.0 g/L of ammonium chloride, 1.80 ml/L of  
538 10 N sodium hydroxide, 10.0 ml of glycerol 0.05% Tween 80 and 0.05 g of ferric  
539 ammonium citrate adjusted to pH 6.6.

540

541

542

543

544

545

546

547

548

549

550

551

552

553

554

555

556

557

558

559

560

## 561 **Figure Legends**

### 562 **Figure 1: X-ray crystal structure of FMN and CTP bound MsmCoaBC.**

563 (A) Full aspect of the dodecameric CoaBC with CoaC represented in teal and CoaB in  
564 gold. (B) View of a CoaBC dimer with FMN and CTP shown. Each protomer is coloured  
565 differently. The CoaC active site flexible flap is highlighted in blue. (C) In the left panel,  
566 a CoaBC trimer is shown with the CoaC coloured in teal and CoaB in gold. On the right  
567 panel dimerization of two CoaBC trimers is shown with CoaC coloured in teal or grey for  
568 different trimers. Each CoaB forms a dimer with protomers from different trimers.

569

### 570 **Figure 2: Detailed view of MsmCoaBC active sites and MsmCoaB dimerisation** 571 **interface.**

572 (A) View of CoaC active site with FMN bound. The active site sits between two  
573 protomers of one trimer (gold and red) and a third protomer from an adjacent trimer  
574 (green). Hydrogen bonds are depicted in yellow and  $\pi$ -interactions are in blue. (B)

575 Superposition of a CoaB crystal structure (PDB code: 6TH2) in green, with full length  
576 CoaBC (teal) showing the active site flaps (brown) of the CoaB and CoaC enzymes. (C)  
577 Detailed view of the CTP binding site. Cartoon and residues belonging to each protomer  
578 are coloured differently. Hydrogen bonds and  $\pi$ -interactions are coloured as in B.  
579 Important waters are represented as red spheres and calcium as a green sphere. Calcium  
580 coordination is depicted in purple. (D) CoaB dimerization interface. Each protomer is  
581 coloured as in C. (D)

582

583 **Figure 3: Regulation of MtbCoaBC by CoA and CoA thioesters.**

584 (A) Inhibition of MtbCoaBC by CoA, acetyl-CoA, malonyl-CoA and succinyl-CoA. (B)  
585 Lineweaver-Burk plots showing the effect of varying the concentration of each substrate  
586 in the presence of different concentrations of acetyl-CoA.

587

588 **Figure 4: Inhibition of MtbCoaBC by compounds 1b and 2b.**

589 (A) Dose response profiles and chemical structure of compounds **1b** and **2b** is shown. (B)  
590 Lineweaver-burke plots showing the effect of varying concentrations of compound **1b**  
591 (left) and **2b** (right) in the presence of varying concentrations of CTP, PPA and L-  
592 cysteine.

593

594 **Figure 5: MsmCoaB X-ray structure showing the cryptic allosteric site.**

595 CoaB with the cryptic allosteric site closed (A) and opened conformation (B) with  
596 compound **1b** (pink) bound. (C) Detailed view of the allosteric site with compound **1b**  
597 (yellow) bound. The individual protomers of the CoaB dimer are coloured in green or  
598 pink.. Hydrogen bonds are depicted in red,  $\pi$ -interactions are in grey, and hydrophobic  
599 interaction in green. Important waters are represented as red spheres and calcium as a



600 green sphere. Calcium coordination is depicted in purple. (D) Gating mechanism of the  
601 cryptic allosteric site showing the movement of R207 with the closed conformation in  
602 yellow and the open conformation in pink. An *E. coli* structure (PDB code: 1U7Z) with  
603 the 4'-phosphopantothenoyl-CMP (purple) intermediate bound is superimposed.

604

605 **Figure 6: Docking of compound 2b into MsmCoaB showing the highest scoring pose.**

606 Hydrogen bonds are shown in red. The individual protomers of the CoaB dimer are either  
607 coloured in green or pink.

608

609

610

611

612 **Tables**

613

614 **Table 1:** Inhibition of CoaB domain by CoA, CoA thioesters and the most potent  
615 inhibitors from of series one and two. IC<sub>50</sub> values determined using the EnzChek  
616 pyrophosphate assay are shown.

<b>Compound</b>	<b>IC<sub>50</sub> EnzCheck (<math>\mu</math>M)</b>
<b>CoA</b>	148 $\pm$ 11
<b>AcCoA</b>	121 $\pm$ 9
<b>MICoA</b>	49 $\pm$ 3
<b>SucCoA</b>	38 $\pm$ 2
<b>1b</b>	0.28 $\pm$ 0.05
<b>1c</b>	4.6 $\pm$ 0.4
<b>2b</b>	0.08 $\pm$ 0.01
<b>2c</b>	0.41 $\pm$ 0.03
<b>2d</b>	0.54 $\pm$ 0.06
<b>2e</b>	3.0 $\pm$ 0.2

617

618 **Table 2:** Minimum inhibitory concentration (MIC) values of CoaB inhibitors against *M.*  
619 *tuberculosis* H37Rv cultured in different media ( $\mu$ M).

Compound	7H9/ADC/ Glycerol	7H9/ Cholesterol/ Tyloxapol	GAST/ Fe
<b>1b</b>	>250	>250	125
<b>1c</b>	>250	ND	ND
<b>2b</b>	>250	>250	50
<b>2c</b>	>250	>250	125
<b>2d</b>	>250	>250	ND
<b>2e</b>	>250	ND	ND

620 \*ND – Not determined.

621

622

623

624

625

## 626 **Acknowledgements**

627 This work was funded by the Bill and Melinda Gates Foundation HIT-TB (OPP  
628 OPP1024021) and SHORTEN-TB (OPP1158806) (VMendes and JCE) and in part by the  
629 Intramural Research Program of NIH, NIAID (HIMB and CEB) and the South African  
630 Medical Research Council and National Research Foundation (VMizrahi). CS was  
631 funded in part by a NHMRC Overseas Biomedical Fellowship (1016357) with support  
632 from the Bill and Melinda Gates Foundation HIT-TB (OPP OPP1024021). CoaBC  
633 screening was funded by a MRC-CinC (grant no. MC\_PC\_14099). TLB is funded by the  
634 Wellcome Trust (Wellcome Trust Investigator Award 200814\_Z\_16\_Z: RG83114). The  
635 authors would like to thank the Diamond Light Source for beam-time (proposals mx9537,  
636 mx14043, mx18548) and the Seattle Structural Genomics Consortium for kindly  
637 providing the *M. smegmatis* CoaB plasmid.

638

## 639 References

- 640 1. World Health, O. *Global tuberculosis report 2019*, (World Health Organization, Geneva,  
641 2019).
- 642 2. Strauss, E. Coenzyme A Biosynthesis and Enzymology. *Comprehensive Natural Products*  
643 *li: Chemistry and Biology, Vol 7: Cofactors*, 351-410 (2010).
- 644 3. Leonardi, R. & Jackowski, S. Biosynthesis of Pantothenic Acid and Coenzyme A. *EcoSal*  
645 *Plus* **2**(2007).
- 646 4. Tsuchiya, Y. et al. Protein CoAlation and antioxidant function of coenzyme A in  
647 prokaryotic cells. *Biochem J* **475**, 1909-1937 (2018).
- 648 5. Choudhary, C. et al. Lysine acetylation targets protein complexes and co-regulates  
649 major cellular functions. *Science* **325**, 834-40 (2009).
- 650 6. Beld, J., Sonnenschein, E.C., Vickery, C.R., Noel, J.P. & Burkart, M.D. The  
651 phosphopantetheinyl transferases: catalysis of a post-translational modification crucial  
652 for life. *Nat Prod Rep* **31**, 61-108 (2014).
- 653 7. Wang, M. & Casey, P.J. Protein prenylation: unique fats make their mark on biology.  
654 *Nat Rev Mol Cell Biol* **17**, 110-22 (2016).
- 655 8. Bird, J.G. et al. The mechanism of RNA 5' capping with NAD<sup>+</sup>, NADH and desphospho-  
656 CoA. *Nature* **535**, 444-7 (2016).
- 657 9. Marrakchi, H., Laneelle, M.A. & Daffe, M. Mycolic acids: structures, biosynthesis, and  
658 beyond. *Chem Biol* **21**, 67-85 (2014).
- 659 10. Guerrini, V. et al. Storage lipid studies in tuberculosis reveal that foam cell biogenesis  
660 is disease-specific. *PLoS Pathog* **14**, e1007223 (2018).
- 661 11. Peyron, P. et al. Foamy macrophages from tuberculous patients' granulomas  
662 constitute a nutrient-rich reservoir for M. tuberculosis persistence. *PLoS Pathog* **4**,  
663 e1000204 (2008).
- 664 12. Evans, J.C. et al. Validation of CoaBC as a Bactericidal Target in the Coenzyme A  
665 Pathway of Mycobacterium tuberculosis. *ACS Infect Dis* **2**, 958-968 (2016).
- 666 13. Kupke, T. et al. Molecular characterization of lantibiotic-synthesizing enzyme EpiD  
667 reveals a function for bacterial Dfp proteins in coenzyme A biosynthesis. *J Biol Chem*  
668 **275**, 31838-46 (2000).
- 669 14. White, M.D. et al. UbiX is a flavin prenyltransferase required for bacterial ubiquinone  
670 biosynthesis. *Nature* **522**, 502-6 (2015).
- 671 15. Blaesse, M., Kupke, T., Huber, R. & Steinbacher, S. Crystal structure of the peptidyl-  
672 cysteine decarboxylase EpiD complexed with a pentapeptide substrate. *EMBO J* **19**,  
673 6299-310 (2000).
- 674 16. Blaesse, M., Kupke, T., Huber, R. & Steinbacher, S. Structure of MrsD, an FAD-binding  
675 protein of the HFCD family. *Acta Crystallogr D Biol Crystallogr* **59**, 1414-21 (2003).
- 676 17. Albert, A. et al. The X-ray structure of the FMN-binding protein AtHal3 provides the  
677 structural basis for the activity of a regulatory subunit involved in signal transduction.  
678 *Structure* **8**, 961-9 (2000).
- 679 18. Manoj, N. & Ealick, S.E. Unusual space-group pseudosymmetry in crystals of human  
680 phosphopantothenoylcysteine decarboxylase. *Acta Crystallogr D Biol Crystallogr* **59**,  
681 1762-6 (2003).
- 682 19. Steinbacher, S. et al. Crystal structure of the plant PPC decarboxylase AtHAL3a  
683 complexed with an ene-thiol reaction intermediate. *J Mol Biol* **327**, 193-202 (2003).
- 684 20. Stanitzek, S., Augustin, M.A., Huber, R., Kupke, T. & Steinbacher, S. Structural basis of  
685 CTP-dependent peptide bond formation in coenzyme A biosynthesis catalyzed by  
686 *Escherichia coli* PPC synthetase. *Structure* **12**, 1977-88 (2004).

- 687 21. Manoj, N., Strauss, E., Begley, T.P. & Ealick, S.E. Structure of human  
688 phosphopantothoenoylcysteine synthetase at 2.3 Å resolution. *Structure* **11**, 927-36  
689 (2003).
- 690 22. Zheng, P. et al. Crystallographic Analysis of the Catalytic Mechanism of  
691 Phosphopantothoenoylcysteine Synthetase from *Saccharomyces cerevisiae*. *J Mol Biol*  
692 (2019).
- 693 23. Kupke, T. Molecular characterization of the 4'-phosphopantothoenoylcysteine  
694 synthetase domain of bacterial dfp flavoproteins. *J Biol Chem* **277**, 36137-45 (2002).
- 695 24. Chan, D.S.-H. et al. Structural insights into *Escherichia coli*  
696 phosphopantothoenoylcysteine synthetase by native ion mobility–mass spectrometry.  
697 *Biochemical Journal* **476**, 3125-3139 (2019).
- 698 25. Strauss, E., Kinsland, C., Ge, Y., McLafferty, F.W. & Begley, T.P.  
699 Phosphopantothoenoylcysteine synthetase from *Escherichia coli*. Identification and  
700 characterization of the last unidentified coenzyme A biosynthetic enzyme in bacteria. *J*  
701 *Biol Chem* **276**, 13513-6 (2001).
- 702 26. Awasthy, D. et al. Essentiality and functional analysis of type I and type III  
703 pantothenate kinases of *Mycobacterium tuberculosis*. *Microbiology* **156**, 2691-701  
704 (2010).
- 705 27. Song, W.J. & Jackowski, S. Kinetics and regulation of pantothenate kinase from  
706 *Escherichia coli*. *J Biol Chem* **269**, 27051-8 (1994).
- 707 28. Vallari, D.S., Jackowski, S. & Rock, C.O. Regulation of pantothenate kinase by coenzyme  
708 A and its thioesters. *J Biol Chem* **262**, 2468-71 (1987).
- 709 29. Wubben, T.J. & Mesecar, A.D. Kinetic, thermodynamic, and structural insight into the  
710 mechanism of phosphopantetheine adenylyltransferase from *Mycobacterium*  
711 *tuberculosis*. *J Mol Biol* **404**, 202-19 (2010).
- 712 30. Miller, J.R. et al. Phosphopantetheine adenylyltransferase from *Escherichia coli*:  
713 investigation of the kinetic mechanism and role in regulation of coenzyme A  
714 biosynthesis. *J Bacteriol* **189**, 8196-205 (2007).
- 715 31. Bennett, B.D. et al. Absolute metabolite concentrations and implied enzyme active site  
716 occupancy in *Escherichia coli*. *Nat Chem Biol* **5**, 593-9 (2009).
- 717 32. Moolman, W.J., de Villiers, M. & Strauss, E. Recent advances in targeting coenzyme A  
718 biosynthesis and utilization for antimicrobial drug development. *Biochem Soc Trans* **42**,  
719 1080-6 (2014).
- 720 33. Kupke, T. Active-site residues and amino acid specificity of the bacterial 4'-  
721 phosphopantothoenoylcysteine synthetase CoaB. *Eur J Biochem* **271**, 163-72 (2004).
- 722 34. Yun, M. et al. Structural basis for the feedback regulation of *Escherichia coli*  
723 pantothenate kinase by coenzyme A. *J Biol Chem* **275**, 28093-9 (2000).
- 724 35. Hartl, J., Kiefer, P., Meyer, F. & Vorholt, J.A. Longevity of major coenzymes allows  
725 minimal de novo synthesis in microorganisms. *Nat Microbiol* **2**, 17073 (2017).
- 726 36. Nguyen, L. & Pieters, J. *Mycobacterium* subversion of chemotherapeutic reagents and  
727 host defense tactics: challenges in tuberculosis drug development. *Annu Rev*  
728 *Pharmacol Toxicol* **49**, 427-53 (2009).
- 729 37. Vonrhein, C. et al. Data processing and analysis with the autoPROC toolbox. *Acta*  
730 *Crystallogr D Biol Crystallogr* **67**, 293-302 (2011).
- 731 38. Kabsch, W. Xds. *Acta Crystallogr D Biol Crystallogr* **66**, 125-32 (2010).
- 732 39. Evans, P.R. & Murshudov, G.N. How good are my data and what is the resolution? *Acta*  
733 *Crystallographica Section D-Biological Crystallography* **69**, 1204-1214 (2013).
- 734 40. French, S. & Wilson, K. Treatment of Negative Intensity Observations. *Acta*  
735 *Crystallographica Section A* **34**, 517-525 (1978).
- 736 41. Winn, M.D. et al. Overview of the CCP4 suite and current developments. *Acta*  
737 *Crystallogr D Biol Crystallogr* **67**, 235-42 (2011).

- 738 42. McCoy, A.J. et al. Phaser crystallographic software. *J Appl Crystallogr* **40**, 658-674  
739 (2007).  
740 43. Adams, P.D. et al. PHENIX: a comprehensive Python-based system for macromolecular  
741 structure solution. *Acta Crystallogr D Biol Crystallogr* **66**, 213-21 (2010).  
742 44. Emsley, P., Lohkamp, B., Scott, W.G. & Cowtan, K. Features and development of Coot.  
743 *Acta Crystallogr D Biol Crystallogr* **66**, 486-501 (2010).  
744 45. Jubb, H.C. et al. Arpeggio: A Web Server for Calculating and Visualising Interatomic  
745 Interactions in Protein Structures. *J Mol Biol* **429**, 365-371 (2017).  
746 46. Singh, V. et al. The complex mechanism of antimycobacterial action of 5-fluorouracil.  
747 *Chem Biol* **22**, 63-75 (2015).

748

749

#### 750 **Author contributions**

751 VMendes wrote the manuscript. VM designed and performed all the crystallographic  
752 experiments with the help of MB, OB and JCW. VMendes and JH designed and  
753 performed the kinetic experiments. JH synthesised 4'-phosphopantothenate. PHMT  
754 performed docking experiments. DSC performed the native mass spectrometry  
755 experiments. SG, TB, SON, SD, JP and CS developed and performed the high-throughput  
756 screening. JCE, SLL and HIMB performed the microbiology experiments on *M.*  
757 *tuberculosis* H37Rv. VMendes, JCE, SG, AGC, PCR, KR, CA, HIMB, CEB, VMizrahi,  
758 PGW and TLB managed the project. All authors approved the manuscript.

759

#### 760 **Accession numbers**

761 Coordinates and structure factors related to this work have been deposited in the PDB  
762 with accession numbers: **6TGV**, **6TH2** and **6THC**.



Figure 2

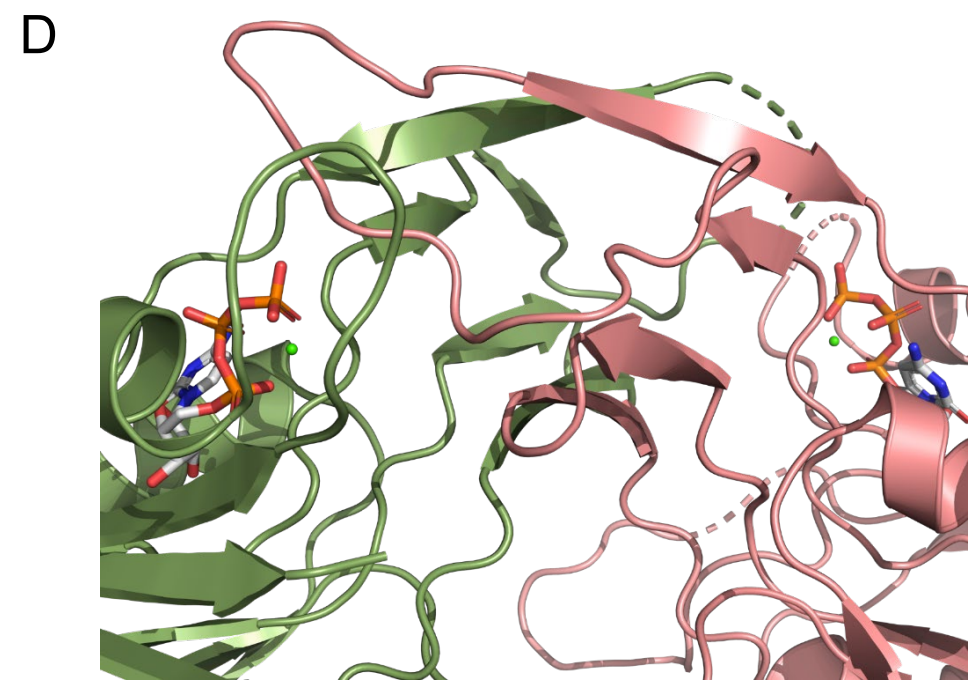
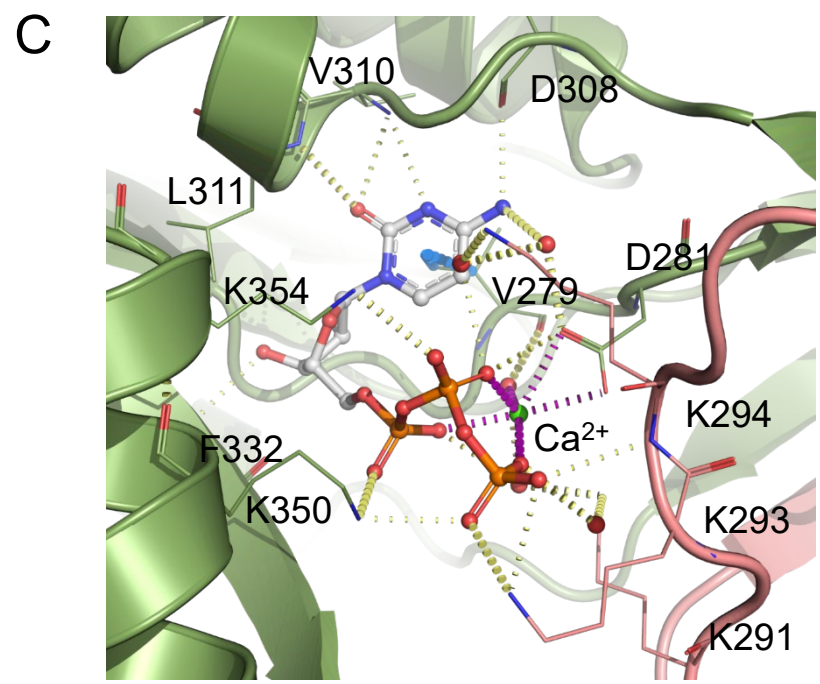
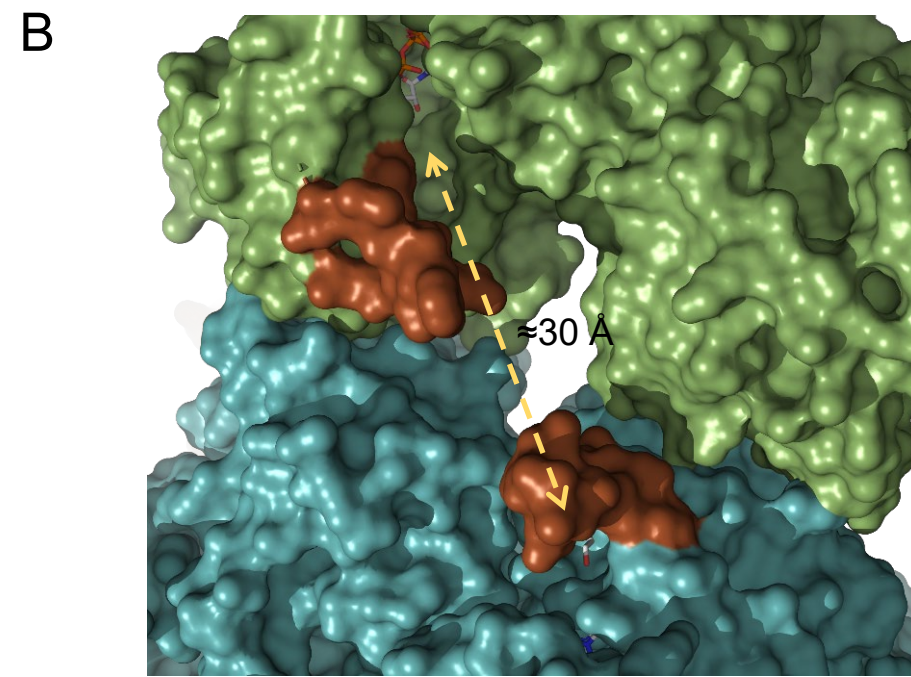
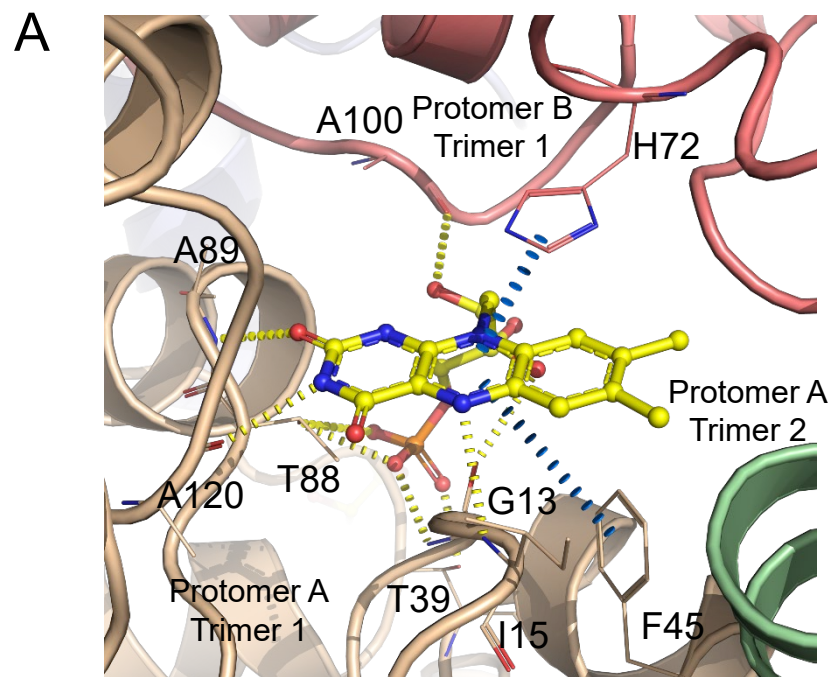
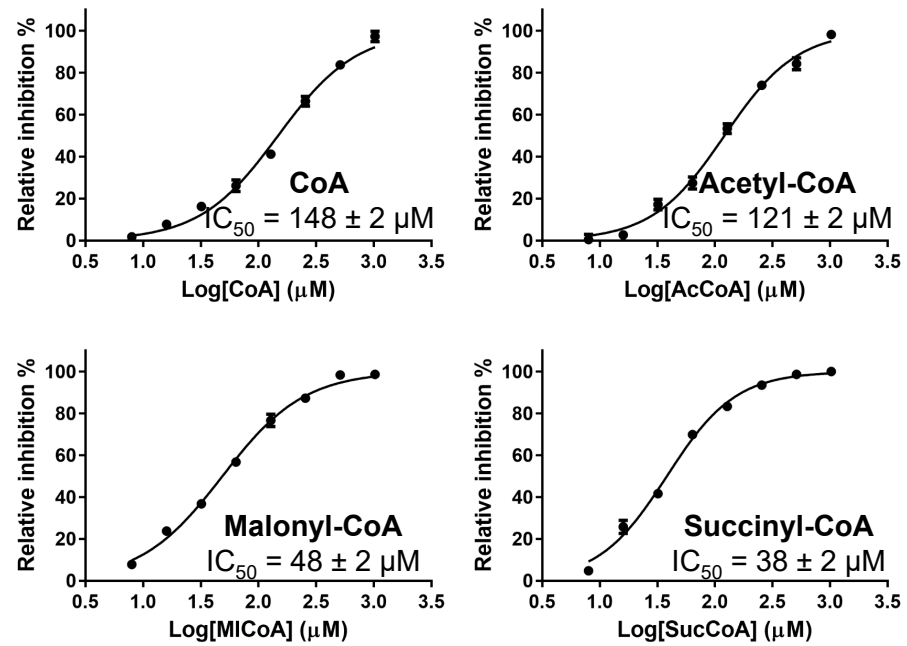


Figure 3

A



B

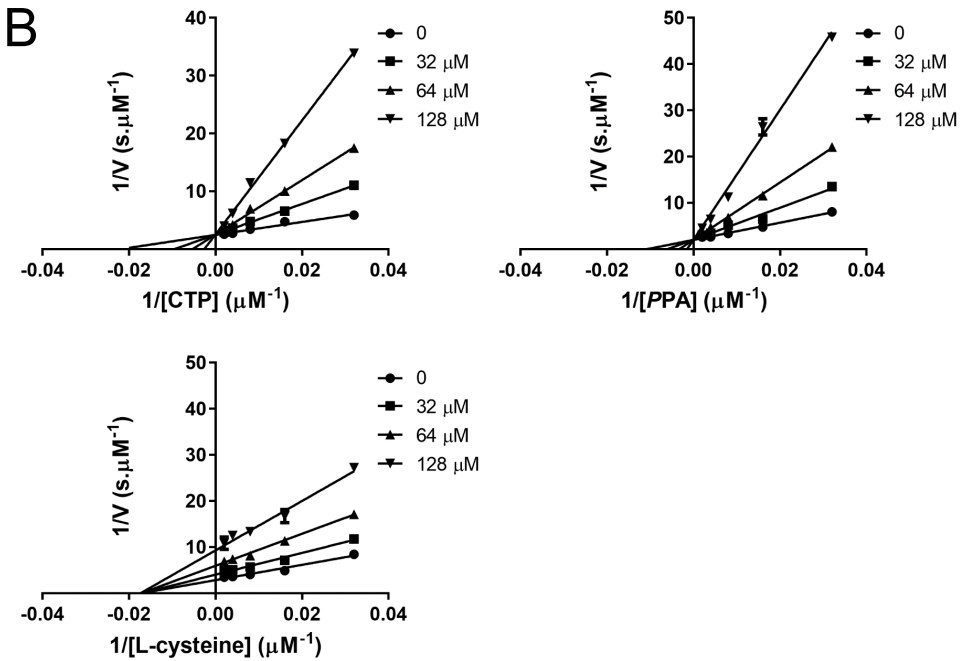
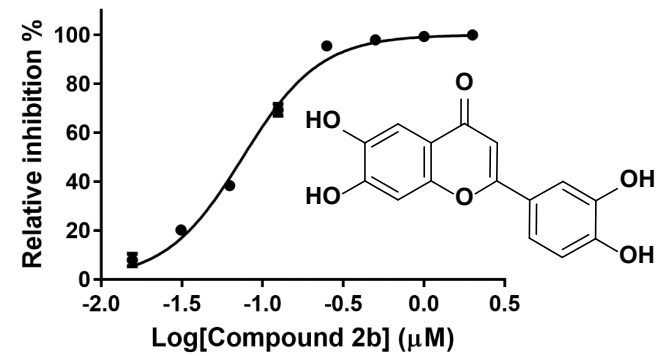
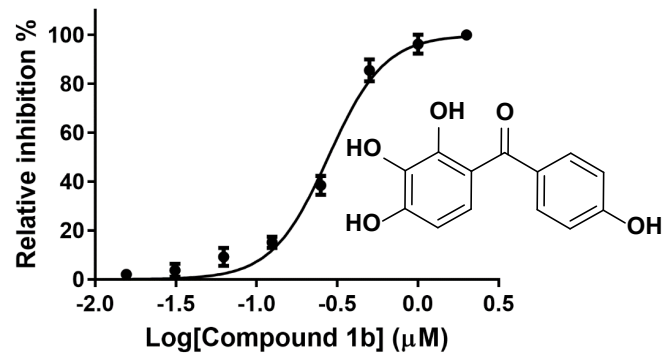


Figure 4

A



B

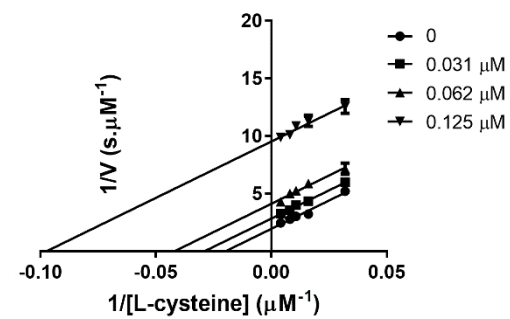
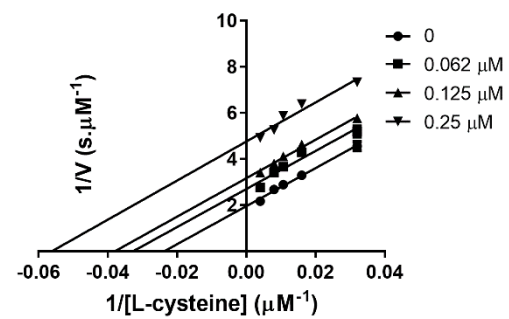
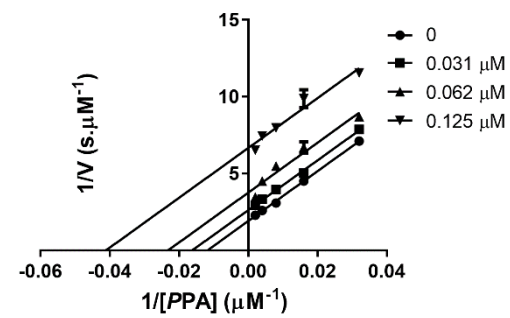
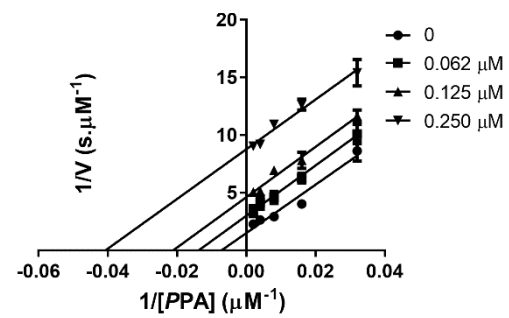
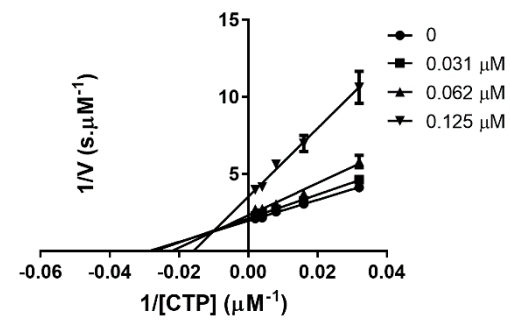
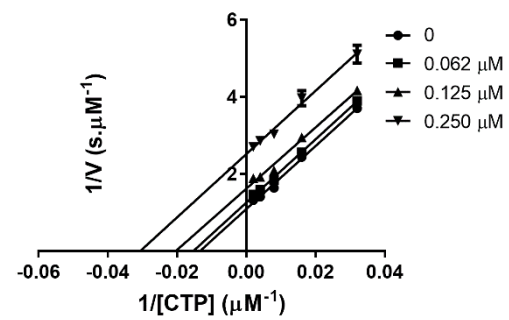




Figure 5

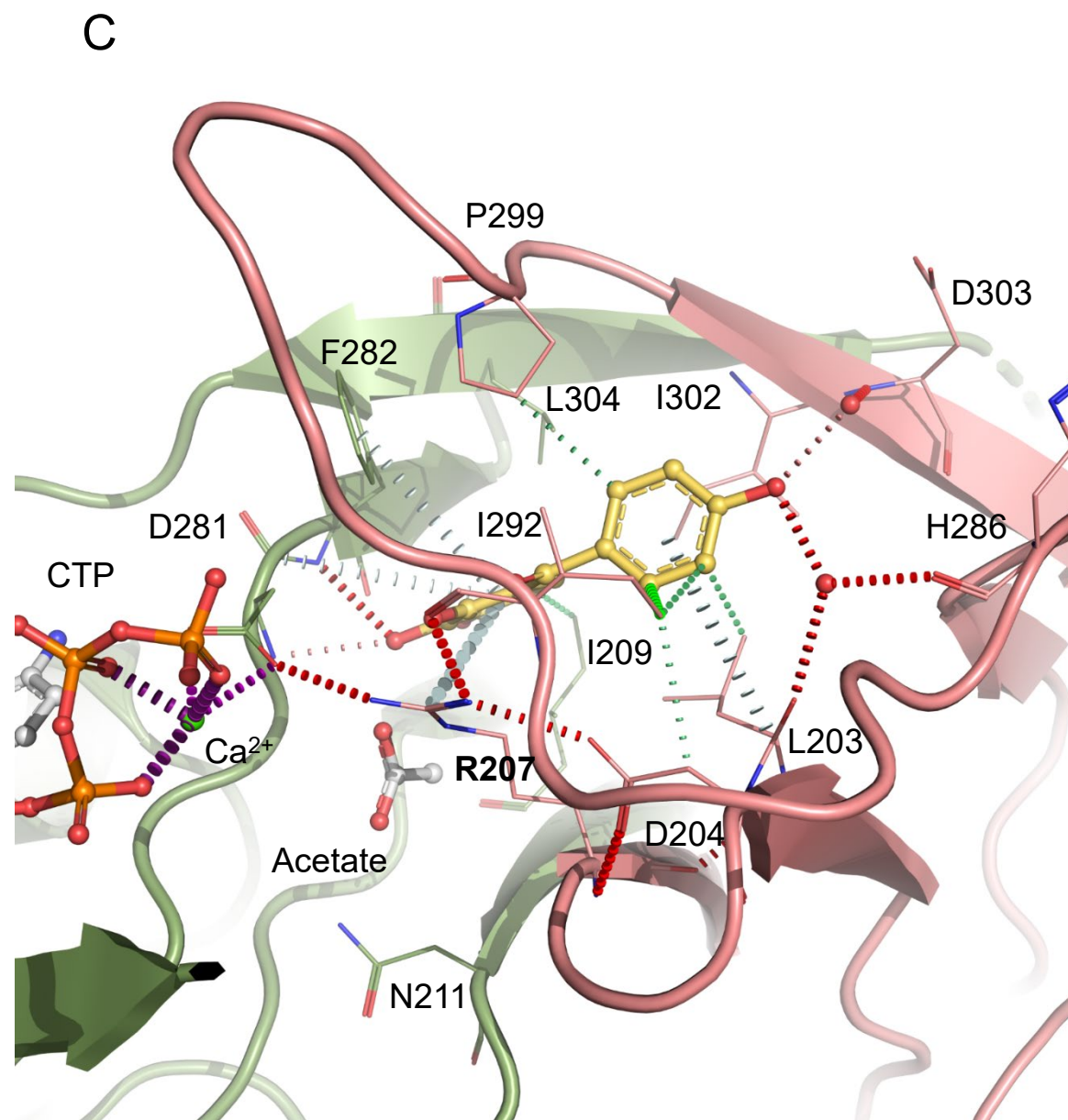
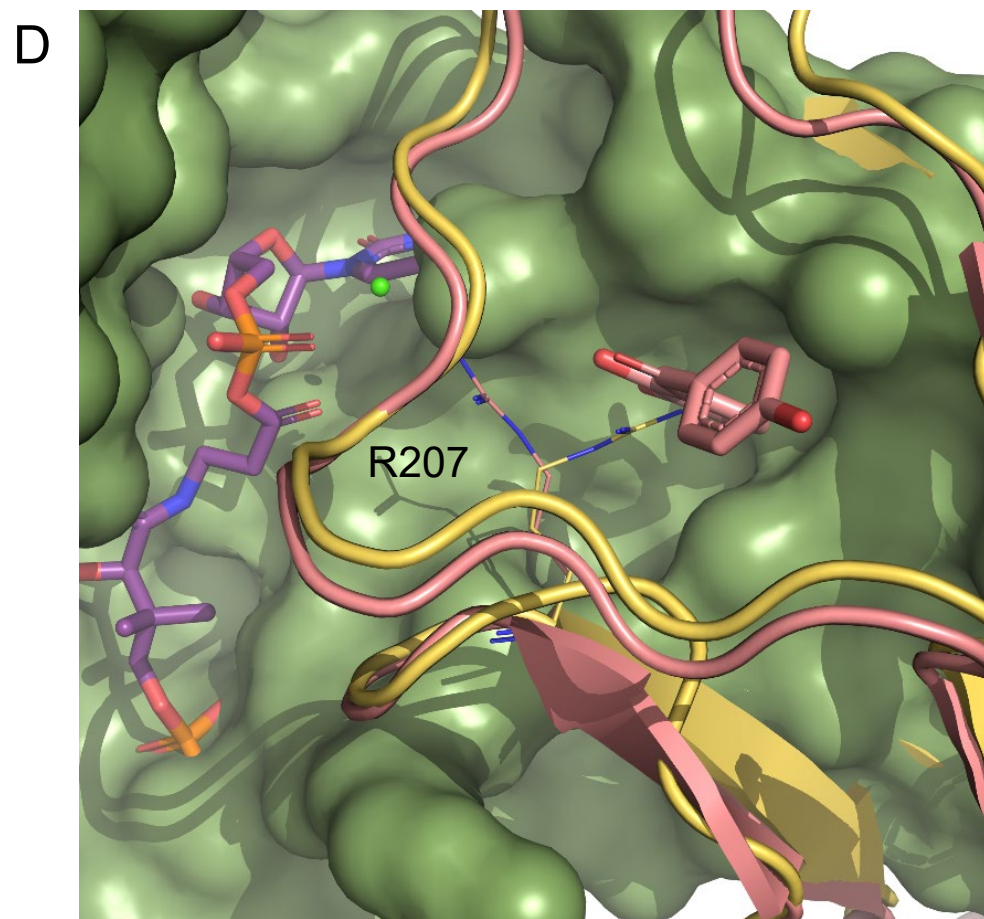
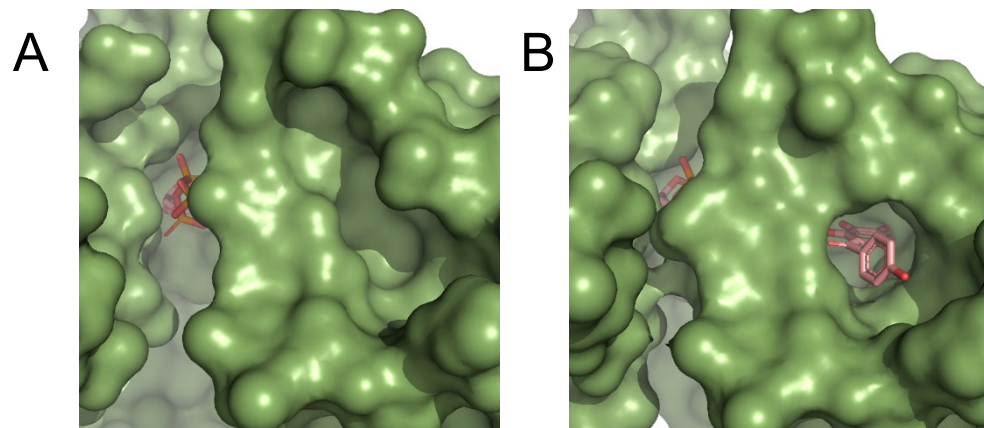


Figure 6

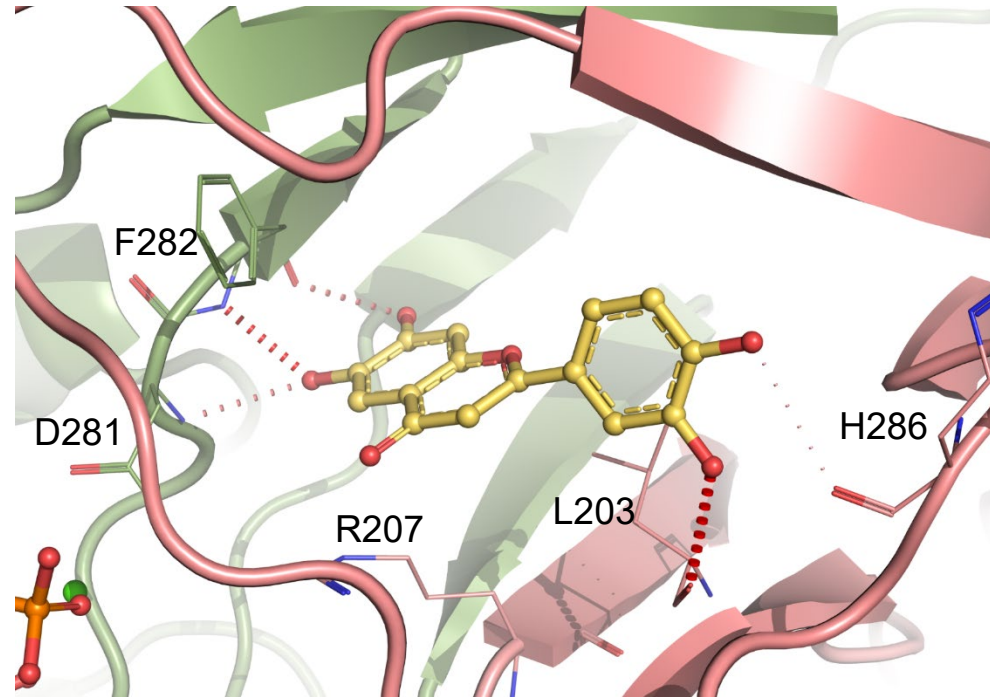
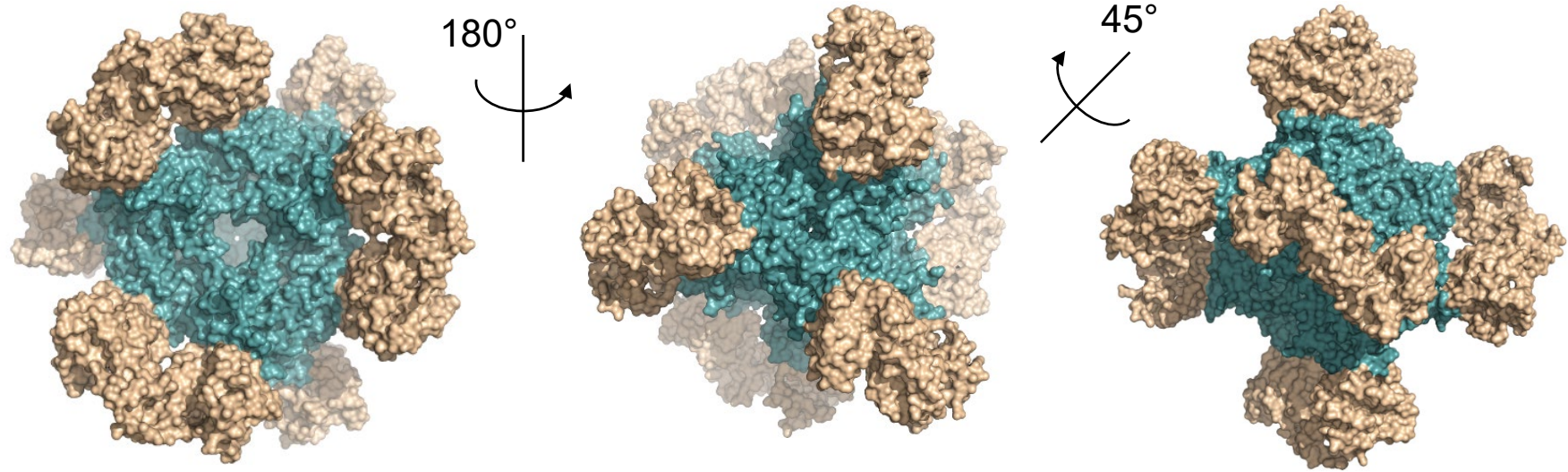


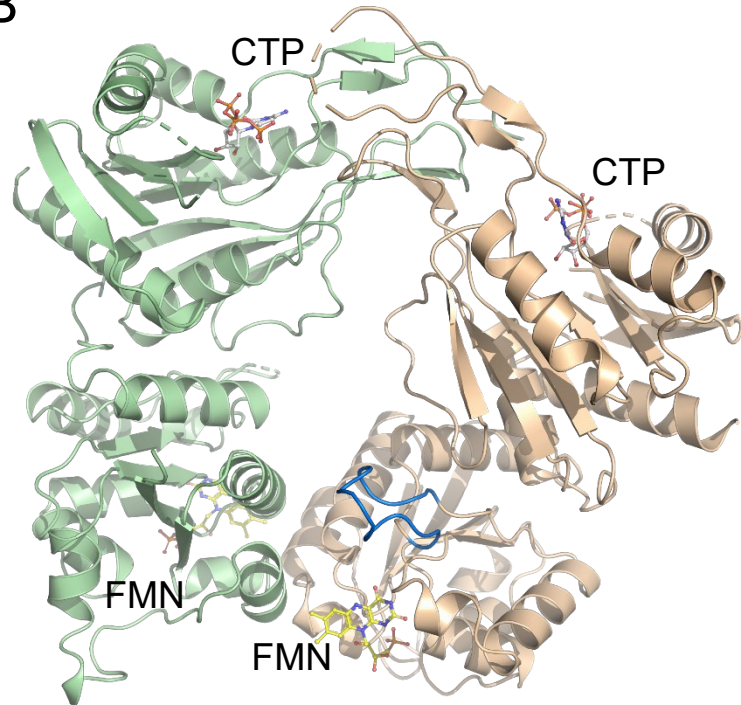


Figure 1

A



B



C

